Effect of excluded volume interactions on the interfacial properties of colloid-polymer mixtures

Andrea Fortini[a)]
Soft Condensed Matter, Debye Institute for NanoMaterials Science, Utrecht University, Princetonplein 5, 3584 CC Utrecht, The Netherlands

Peter G. Bolhuis
van't Hoff Institute for Molecular Sciences, University of Amsterdam, Nieuwe Achtergracht 166, 1018 WV Amsterdam, The Netherlands

Marjolein Dijkstra
Soft Condensed Matter, Debye Institute for NanoMaterials Science, Utrecht University, Princetonplein 5, 3584 CC Utrecht, The Netherlands

(Received 10 July 2007; accepted 5 November 2007; published online 11 January 2008)

We report a numerical study of equilibrium phase diagrams and interfacial properties of bulk and confined colloid-polymer mixtures using grand canonical Monte Carlo simulations. Colloidal particles are treated as hard spheres, while the polymer chains are described as soft repulsive spheres. The polymer-polymer, colloid-polymer, and wall-polymer interactions are described by density-dependent potentials derived by Bolhuis and Louis [Macromolecules **35**, 1860 (2002)]. We compared our results with those of the Asakura-Oosawa-Vrij model [J. Chem. Phys. **22**, 1255 (1954); J. Polym Sci **33**, 183 (1958); Pure Appl. Chem. **48**, 471 (1976)] that treats the polymers as ideal particles. We find that the number of polymers needed to drive the demixing transition is larger for the interacting polymers, and that the gas-liquid interfacial tension is smaller. When the system is confined between two parallel hard plates, we find capillary condensation. Compared with the Asakura-Oosawa-Vrij model, we find that the excluded volume interactions between the polymers suppress the capillary condensation. In order to induce capillary condensation, smaller undersaturations and smaller plate separations are needed in comparison with ideal polymers. [DOI: 10.1063/1.2818562]

I. INTRODUCTION

Mixtures of colloids and polymers[1–3] are simple model systems that have been studied extensively in the past few years. Provided the size and the number of polymers are sufficiently high, such mixtures can phase separate into a *colloidal gas* phase that is poor in colloids and rich in polymers and a *colloidal liquid* phase that is rich in colloids and poor in polymers. While it is well established that the interactions between sterically stabilized colloidal particles are well described by the hard sphere potential,[4] the interactions between the polymers in the mixture can be, in general, very complicated. Nevertheless, if we consider the case of flexible polymer chains in a "good solvent" conditions, we can assume that the excluded volume interactions between the chains are small and that the chains cannot penetrate the colloidal particles. The mechanism behind the demixing transition is then easily explained. In Fig. 1(a), we illustrate the mixture of spherical colloids and polymer chains. Around each colloid, there is a depletion region prohibited to the polymers due to the hard-core interactions. If two colloids approach each other, so that two depletion zones overlap, there is an increase in free volume for the polymer chains, i.e., an increase in entropy. The increase in entropy can be described by an effective attractive interaction between the colloidal particles. A similar depletion mechanism occurs between a hard wall and the colloidal particles. If the polymers do not adsorb at the wall, they are excluded from a region close to the wall. The overlap between the depletion zone at the wall and the depletion zone of one colloid induces an increase in free volume and, hence, in entropy.

One particular simple model for colloid-polymer mixtures is the Asakura-Oosawa-Vrij (AOV) model[5–7] that describes the polymer chains as spherical particles with a radius equal to the radius of gyration of the polymer. Furthermore, polymer spheres can freely overlap, while they are excluded from a center of mass distance from the colloidal particles. The AOV model has been studied extensively in the past few years, and it was shown that it describes qualitatively the bulk[8–16] and interfacial phase behavior[17–22] of mixtures of colloids and polymers. A similar level of agreement was found for the interfacial tension of the gas-liquid[16,23,24] and wall-fluid interfaces,[24–26] and for the phase behavior of confined systems.[27–34]

The quantitative discrepancies between experimental results and the AOV model results can arise from a number of reasons, such as nonideal solvent conditions,[35] colloid-induced polymer compression,[36] effect of charges on the colloidal surface,[37,38] or polymer excluded volume interactions.

[a)]Present address: Department of Physics, Yeshiva University, 500 West 185th Street, New York, NY 10033, USA. Electronic mail: a.fortini@phys.uu.nl.

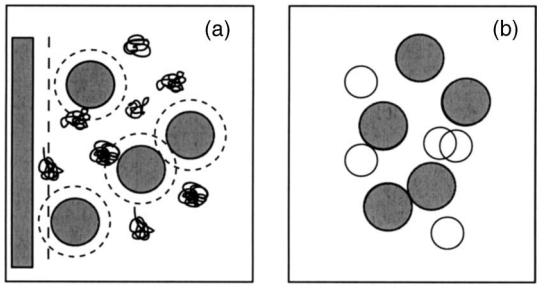

FIG. 1. (a) Illustration of a mixture of colloids and polymer chains in contact with a hard wall. Depletion zones (dashed lines) and overlap zones (light gray) are also depicted. (b) Illustration of a model colloid-polymer mixture in the polymer-as-soft-sphere approach.

In this article, we will concentrate on the latter aspect. The simplest inclusion of polymer interactions was done by introducing a step function interaction between the polymers, i.e., an energy penalty for the overlaps of two polymers. The step potential was used to study the bulk phase diagram and interfacial tension[25,39,40] as well as the stability of the floating liquid phase in sedimenting colloid-polymer mixtures[41] with a geometry-based density functional theory (DFT). This approach gives results that are in better agreement with experiments when compared against the AOV model, but the height of the step potential must be introduced as an additional free parameter. Furthermore, we expect the polymer-colloid interaction to be modified as well when considering excluded volume interactions between polymers. Other theoretical approaches have been developed to study the effect of polymer interactions in colloid-polymer mixtures. Aarts *et al.*[42] extended the free volume theory[9] to include polymer interactions and studied the gas-liquid interfacial tension with the square gradient approximation approach.[42–45] A one-component perturbative DFT that includes excluded volume interactions and uses the approach of Ref. 46 was developed by Moncho-Jorda *et al.*[47] to study confined systems and the gas-liquid tension.

Another approach is to describe the polymers as soft spheres,[48–50] with effective interactions derived from inversion of the center of mass correlation functions in lattice self-avoiding-walk (SAW) polymer simulations. This approach generates soft density-dependent potentials for the polymer-polymer and colloid-polymer interactions, which gives accurate simulation results for the bulk phase behavior[51] that are in quantitative agreement with experimental results. In a similar approach, proposed by Jusufi *et al.*,[52] the effective potentials are derived from off-lattice molecular dynamics simulations of SAW polymer chains. These potentials were used in Monte Carlo simulations to study the bulk phase behavior[53,54] and the gas-liquid interfacial tension[55] of colloid-polymer mixtures, leading to results in quantitative agreement with experiments.

In this work, we study the effect of excluded volume interactions on the interfacial properties and phase behavior of confined colloid-polymer mixtures with Monte Carlo simulations. We simulate a binary mixture with the density-dependent potentials derived in Ref. 48 and compare the simulation results with those for the AOV model.

TABLE I. Coefficients for the density-dependent parameters of the polymer-polymer interaction potential v_{pp} defined in Eq. (2).

	$k=1$	$k=2$	$k=3$
a_k^0	1.474 09	−0.232 10	0.638 97
a_k^1	−0.076 89	0.031 32	0.241 93
b_k^0	0.981 37	0.421 23	⋯
b_k^1	−0.056 81	−0.026 28	⋯

II. MODEL

The colloids are treated as hard spheres and the corresponding pair potential reads

$$\beta v_{cc}(R_{ij}) = \begin{cases} \infty & \text{if } r_{ij} < \sigma_c \\ 0 & \text{otherwise,} \end{cases} \tag{1}$$

where $R_{ij}=|\mathbf{R}_i-\mathbf{R}_j|$ is the distance between two colloidal particles, with $\mathbf{R}_i$ the position of the center of mass of colloid i, $\beta \equiv 1/k_BT$, k_B is Boltzmann's constant, and T the temperature. For the coarse-grained effective polymer-polymer, colloid-polymer, and wall-polymer potentials, we use the expressions of Ref. 48 obtained from microscopic simulations of SAW polymer chains consisting of 500 segments on a lattice and a radius of gyration $R_g=16.83$ lattice units at zero concentration. We introduce the overlap concentration ρ^* defined by the equation $4/3\pi\rho^* R_g^3=1$ and the polymer reservoir packing fraction $\eta_p^r=p_p^r/\rho^*$, with ρ_p^r the density in the reservoir of pure polymers in osmotic equilibrium with the two-component system of interest.

The effective density-dependent polymer-polymer interactions[48] read

$$\beta v_{pp}(r_{ij}, \eta_p^r) = \sum_{k=1}^{3} a_k(\eta_p^r)\exp[(-r_{ij}/(R_g b_k(\eta_p^r)))^2], \tag{2}$$

where R_g is the radius of gyration and $r_{ij}=|\mathbf{r}_i-\mathbf{r}_j|$ is the distance between two polymers, with $\mathbf{r}_i$ the position of the center of mass of polymer i. The density-dependent parameters are linear in the density, $a_k=a_k^0+a_k^1\eta_p^r$ and $b_k=b_k^0+b_k^1\eta_p^r$. All coefficients, except b_k^3, are given in Table I. The coefficients b_k^3 are fixed by imposing the equality of the mean field equation of state,

$$\beta P/\rho_p = 1 + \rho_p \beta \hat{v}(0;\rho_p)/2, \tag{3}$$

for the fitted potentials and the SAW simulations, where the function

$$\beta \hat{v}(0;\rho_p) = 4\pi \int r^2 \beta v_{pp}(r,\rho_p) dr \tag{4}$$

is the $k=0$ component of the Fourier transform of the polymer-polymer pair potential. In practice, the condition is satisfied by imposing the equality between

$$\beta \hat{v}(0;\eta_p^r) = \pi^{3/2} \sum_{i=1}^{3} a_i(\eta_p^r) b_i(\eta_p^r)^3 \tag{5}$$

derived from Eq. (2) and

TABLE II. Coefficients for the density-dependent parameters of the colloid-polymer interaction potential v_{cp} defined in Eq. (7) for size ratio q=1.05.

	$k=1$	$k=2$
c_k^0	5.5610	1.8477
c_k^1	−0.8042	1.4759
d_k^0	0.7751	1.2720
d_k^1	−0.1151	0.1052
e_k^0	0.4082	0.0
e_k^1	0.1410	0.0

$$\beta\hat{v}(0;\eta_p^r) = 4\pi(1.2902 + 0.281\,32\eta_p^r + 0.136\,76(\eta_p^r)^2 - 0.040\,892(\eta_p^r)^3) \quad (6)$$

derived using the potentials obtained from the inversion of the radial distribution function determined from SAW simulations.

The concentration-dependent colloid-polymer potential reads[51]

$$\beta v_{\mathrm{cp}}(|\mathbf{R}_i - \mathbf{r}_j|, \eta_p^r) = \sum_{k=1}^{2} c_k(\eta_p^r)\exp[-((|\mathbf{R}_i - \mathbf{r}_j| - e_k(\eta_p^r))/(R_g d_k(\eta_p^r)))^2], \quad (7)$$

where $|\mathbf{R}_i - \mathbf{r}_j|$ is the distance between colloid i and polymer j. The density-dependent parameters are linear in density, i.e., $c_k = c_k^0 + c_k^1\eta_p^r$, $d_k = d_k^0 + d_k^1\eta_p^r$, and $e_k = e_k^0 + e_k^1\eta_p^r$. The coefficients are given in Table II for size ratio $q=1.05$.

The interaction between colloidal particles and the hard wall is hard-sphere-like; that is, the colloidal particles cannot penetrate the walls. The interaction between polymers and the hard wall[48] reads

$$\beta v_{\mathrm{wp}}(z,\eta_p^r) = f_0(\eta_p^r)\exp[f_1(\eta_p^r)z/R_g + f_2(\eta_p^r)z^2/R_g^2 + f_3(\eta_p^r)z^3/R_g^3], \quad (8)$$

where z is the distance between the wall and the center of mass of the polymer. The parameters have a quadratic density dependence $f_k(\eta_p^r) = f_k^0 + f_k^1\eta_p^r + f_k^2(\eta_p^r)^2$, with $k=0,1,2,3$. The coefficients are given in Table III. In Fig. 2, we show the effective polymer-polymer, colloid-polymer, and wall-polymer interactions for $\eta_p^r = 1.029\,95$ as an example.

A final note on the potentials described in this section is in order. Due to a small error in the calculation of the radius of gyration in Ref. 48, all the equations and coefficients presented here were parametrized assuming a radius of gyration $R_g = 16.495$ lattice units, instead of the correct value of $R_g = 16.83$. The simulations we carried out for this work, as well as the simulations presented in Ref. 51, were done imposing a size ratio $q=1.03$ (corresponding to the radius of gyration $R_g = 16.495$) in the calculations. All the results have been interpreted using the correct value for the size ratio $q=1.05$ (corresponding to the radius of gyration $R_g = 16.83$). This correction only changes the values of the polymer packing fractions η_p and η_p^r, while the colloid packing fraction η_c is unaffected.

TABLE III. Coefficients for the density-dependent parameters of the wall-polymer interaction potential v_{wp} defined in Eq. (8).

	$k=0$	$k=1$	$k=2$	$k=3$
f_k^0	62.7242	−6.4093	2.5081	−0.6904
f_k^1	56.4595	−3.8880	5.1562	−1.5519
f_k^2	−29.9283	2.0442	−2.1336	0.5973

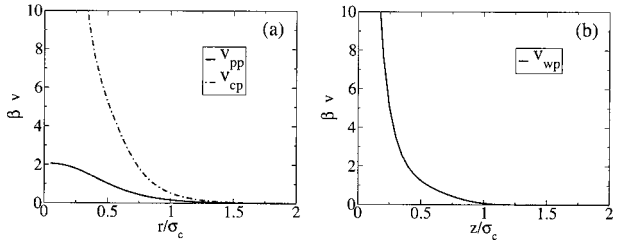

FIG. 2. Interaction potentials for polymer density $\eta_p^r = 1.029\,95$. (a) Pair potential between polymers βv_{pp} (full line) and between polymers and colloids βv_{cp} (dashed line). (b) Wall-polymer potential βv_{wp} as a function of the distance z/σ_c of the polymer center of mass from the wall.

III. METHOD

We carried out Monte Carlo simulations in the grand canonical ensemble, i.e., with fixed volume, temperature, and chemical potentials μ_c and μ_p of colloids and polymers, respectively. For each value of μ_p, we determined the potentials given in the previous section, at the polymer reservoir packing fraction $\eta_p^r(\mu_p)$ calculated by inversion of the equation of state,

$$\frac{\mu_p}{k_BT}R_g^3 = \log(\rho_p^r R_g^3) + 0.046\,58 + 11.05\rho_p^r R_g^3 + 35.48(\rho_p^r R_g^3)^2 - 15.71(\rho_p^r R_g^3)^3. \quad (9)$$

This equation was derived by integrating the Gibbs-Duhem equation with the pressure given by Eqs. (3) and (6).

To study phase coexistence, we sample the probability $P(N_c)|_{z_c,\eta_p^r}$ of observing N_c colloids in a volume V at fixed colloid fugacity z_c and fixed polymer reservoir packing fraction η_p^r, using the successive umbrella sampling.[56] We use the histogram reweighting technique to obtain the probability distribution for any z_c' once $P(N_c)|_{z_c,\eta_p^r}$ is known for a given z_c,

$$\ln P(N_c)|_{z_c',\eta_p^r} = \ln P(N_c)|_{z_c,\eta_p^r} + N_c \ln\left(\frac{z_c'}{z_c}\right). \quad (10)$$

At phase coexistence, the distribution function $P(N_c)$ becomes bimodal with two separate peaks of equal area for the colloidal liquid and gas phases. We determine which z_c' satisfies the equal area rule,

$$\int_0^{\langle N_c\rangle} P(N_c)|_{z_c',\eta_p^r} dN_c = \int_{\langle N_c\rangle}^{\infty} P(N_c)|_{z_c',\eta_p^r} dN_c, \quad (11)$$

with the average number of colloids

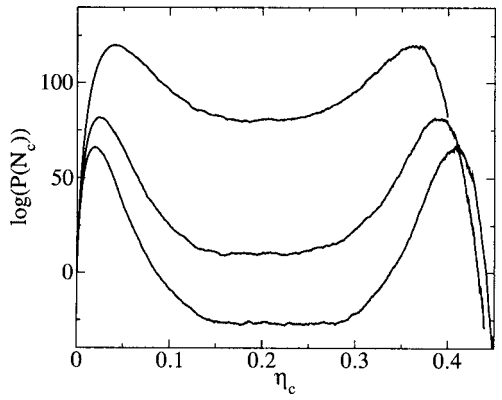

FIG. 3. Logarithm of the probability $P(N_c)$ (not normalized) as a function of the colloid packing fraction η_c for a simulation box with dimensions of $12\times12\times16\sigma^3$ at varying polymer reservoir packing fractions $\eta_p^r=1.14$, 1.20, and 1.23, from top to bottom. All state points are at coexistence.

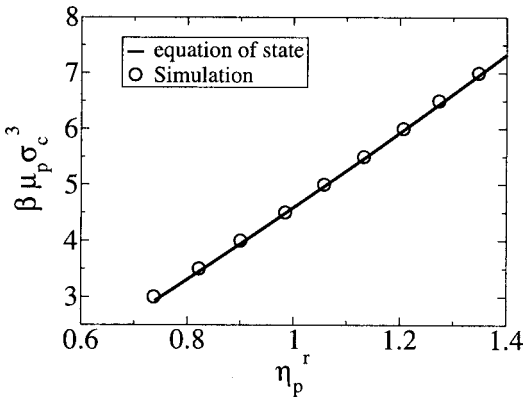

FIG. 4. The chemical potential $\beta\mu_p\sigma_c^3$ as a function of the polymer packing fraction η_p^r in a system of pure polymers. The equation of state (9) (solid line) is compared with the results of grand canonical Monte Carlo simulations (circles) of pure polymers interacting with the interaction potential [Eq. (2)].

$$\langle N_c\rangle = \int_0^\infty N_c P\,(N_c)|_{z_c',\eta_p^r} dN_c, \tag{12}$$

using the histogram reweighting Eq. (10). The simulations are carried out in a rectangular box $V=L\times L\times H$, and the sampling of the probability ratio $P(N)/P(N+1)$ is done, in each window, until the difference between two successive samplings of the probability ratio is smaller than 5×10^{-4}. An example of the sampled probability distributions is given in Fig. 3.

We used single particle insertion/deletion of colloids and polymers. The typical acceptance probabilities for the insertion/deletion of colloids were from 4% to 1% (from low to high colloid density) for state points close to the critical points and from 0.1% to 0.01% at high η_p^r. On the other hand, the acceptance probabilities for the insertion/deletion of polymers were always larger than 40%. The low insertion/deletion probabilities of colloidal particles have only an effect on the efficiency of the algorithm. As shown by the smooth probability distributions in Fig. 3, our simulations were long enough to get good data.

The liquid-gas interfacial tension γ_{lg} is obtained from $P(N_c)|_{z_c',\eta_p^r}$ at coexistence,[57]

$$\gamma_{lg} = \frac{1}{2L^2}\left[\ln\left(\frac{P(N_{c,\max}^g)+P(N_{c,\max}^l)}{2}\right)-\ln(P(N_{c,\min}))\right], \tag{13}$$

where $P(N_{c,\max}^g)$ and $P(N_{c,\max}^l)$ are the maxima of the gas and liquid peaks, respectively, and $P(N_{c,\min})$ is the minimum between the two peaks.

IV. RESULTS

In Sec. II, we explained the straightforward but nontrivial procedure for generating the interaction potentials. It is, therefore, important to check the internal consistency of our calculations. Figure 4 shows the predictions of the equation of state (9) plotted against simulation results of a grand canonical simulation of pure polymers interacting with the potential [Eq. (2)]. In the range of chemical potentials that are relevant for the gas-liquid separation, the simulation results are consistent with the equation of state.

A. Bulk phase behavior and gas-liquid interfacial tension

In Fig. 5, we present the bulk phase diagram obtained from grand canonical Monte Carlo simulations using successive umbrella sampling and histogram reweighting. In particular, Fig. 5(a) shows the phase diagram in the polymer packing fraction η_p, colloid packing fraction η_c representation. These results are consistent with the findings of Ref. 51. The free volume theory[58] extended to include excluded volume polymer interactions[42] overestimates the simulation results by almost a factor of 2. This result may be explained by the renormalization group theory expression used in Ref. 42 to evaluate the polymer interactions, which underestimates the correlation length of the polymers. Since the polymers are effectively smaller, a higher number of polymers is needed to drive the demixing transition. Also shown are the experimental results of de Hoog and Lekkerkerker.[12] The experimental polymer concentration is much larger than those in our simulation results. This discrepancy can be explained by considering the depletion force measurements of Wijting *et al.*[59] in the same colloid-polymer system as was used in Ref. 12. They found that the depletion forces are much smaller than expected, probably due to adsorption of the polymers on the colloidal surface. We stress that the potentials used in this work compare well with the experiments of Ramakrishnan *et al.*[60] at a size ratio $q=0.67$.[51]

Figure 5(b) shows the phase diagram in the polymer reservoir packing fraction η_p^r, colloid packing fraction η_c representation. The discrepancy between our results and those of Ref. 51 is due to a slightly different equation of state used for the conversion of the chemical potential μ_p to the polymer packing fraction in the reservoir η_p^r. In this work, we inverted Eq. (9), while in Ref. 51, the original SAW equation of state was used. The binodal has a critical point at lower η_p^r, and the density difference between the gas and liquid

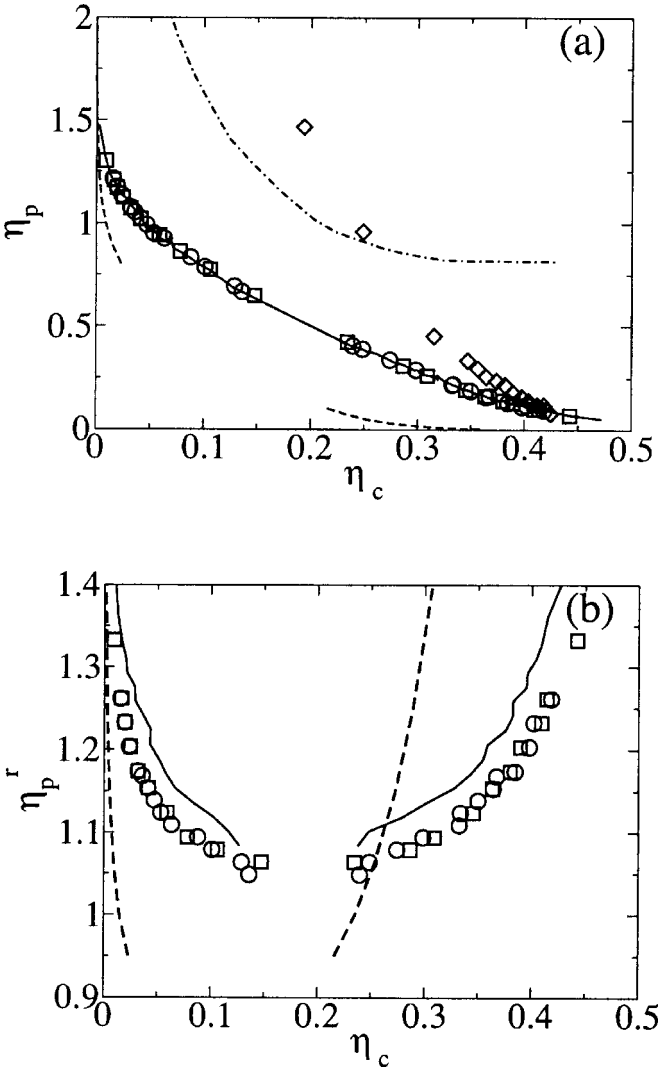

FIG. 5. Bulk phase diagram of colloid-polymer mixtures with a size ratio $q=1.05$ for volumes $V=516\sigma_c^3$ (circles) and $2304\sigma_c^3$ (squares). Also shown are the binodals of the AOV model with size ratio $q=1.0$ (dashed lines) and the results of Ref. 51 (solid line). (a) Polymer packing fraction η_p, colloid packing fraction η_c representation. Shown also are the results of the free volume theory with polymer interactions (Ref. 42) (dotted-dashed line) and the experimental results of de Hoog and Lekkerkerker (Ref. 12) (diamonds). (b) Polymer reservoir packing fraction η_p^r, colloid packing fraction η_c representation.

phases increases for increasing η_p^r. This phase diagram is equivalent to the temperature-density phase diagram of a simple fluid, with the polymer reservoir packing fraction playing the role of inverse temperature.

In Fig. 6, we present the simulation results of the dimensionless interfacial tension $\beta\gamma_{gl}\sigma_c^2$ for the gas-liquid interface, as a function of the difference in packing fractions between the gas and the liquid phase. The interfacial tensions decrease in the case of excluded volume interactions with respect to the AOV model. The comparison between our results and the experiments of Aarts *et al.*[21] is quantitatively better than the results of the AOV model, although de Hoog and Lekkerkerker[12] show that it is difficult to obtain accurate interfacial tension measurements. In addition, we compare our results with the predictions of the extended free volume theory plus a square gradient approximation to evaluate the

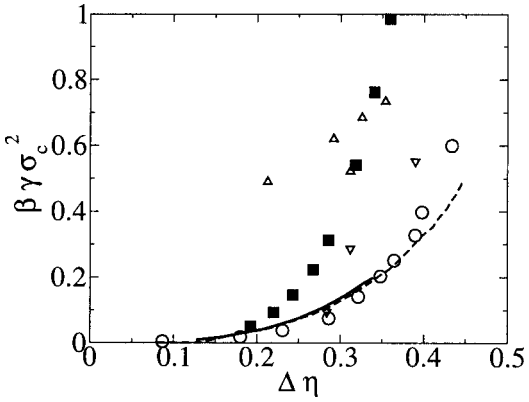

FIG. 6. Dimensionless interfacial tension $\beta\gamma\sigma_c^2$ between the gas and the liquid phase as a function of the difference in packing fractions $\Delta\eta=\eta_l-\eta_g$ of the coexisting liquid (η_l) and gas (η_g) phases. Results for the interacting polymers with size ratio $q=1.05$ (circles) are compared with the results for the AOV model with size ratio $q=1.0$ (square). Triangles denote experimental results of de Hoog and Lekkerkerker (Ref. 12) (triangles up) and Aarts *et al.* (Ref. 21) (triangles down). The thick continuous line indicates the DFT predictions of Moncho-Jorda *et al.* (Ref. 47), while the dashed lines are the predictions of the square gradient approximation theory of Aarts *et al.* (Ref. 45).

tension[45] and the DFT of Moncho-Jorda *et al.*[47] The DFT uses effective one-component pair potentials between the colloids that include the excluded volume interaction according to the approach of Louis *et al.*[46] The predictions of the two theories are very close to each other and to our simulation results.

Figure 7 shows the phase diagram of colloid-polymer mixtures confined between two hard walls with separation distances $H/\sigma_c=\infty,16,8,4,2$. In particular, Fig. 7(a) shows the phase diagram of colloid-polymer mixtures in the polymer packing fraction η_p, colloid packing fraction η_c representation. The binodals in Fig. 7(a) hardly change under confinement. We stress that the comparison between the absolute densities inside capillaries of different sizes is complicated due to two factors. First, the density for confined systems is an ill-defined quantity because it depends on the definition of the volume. Our choice of volume depends on the wall separation. Therefore, the comparison between densities for different wall separations is not entirely consistent. Second, the adsorption of colloids and polymers is different for different wall separations. We find that the colloid adsorption is, in general, larger for larger wall separations and, consequently, the polymer adsorption is smaller. Therefore, for larger wall separations, we expect a larger colloid density and a smaller polymer density. The combination of these two effects renders the interpretation of the phase diagram in the η_p and η_c representation fairly complicated. Figure 7(b) displays the phase diagram of colloid-polymer mixtures in the polymer reservoir packing fraction η_p^r, colloid packing fraction η_c representation. The critical points of the confined systems shift toward higher η_p^r for decreasing wall separation. The interpretation of the binodals in the (η_p^r,η_c) representation is more straightforward because only η_c suffers of the problems described above. We can say that the huge shift in gas densities at coexistence for the confined systems with respect to the bulk binodal is due to the formation of liquid layers at the

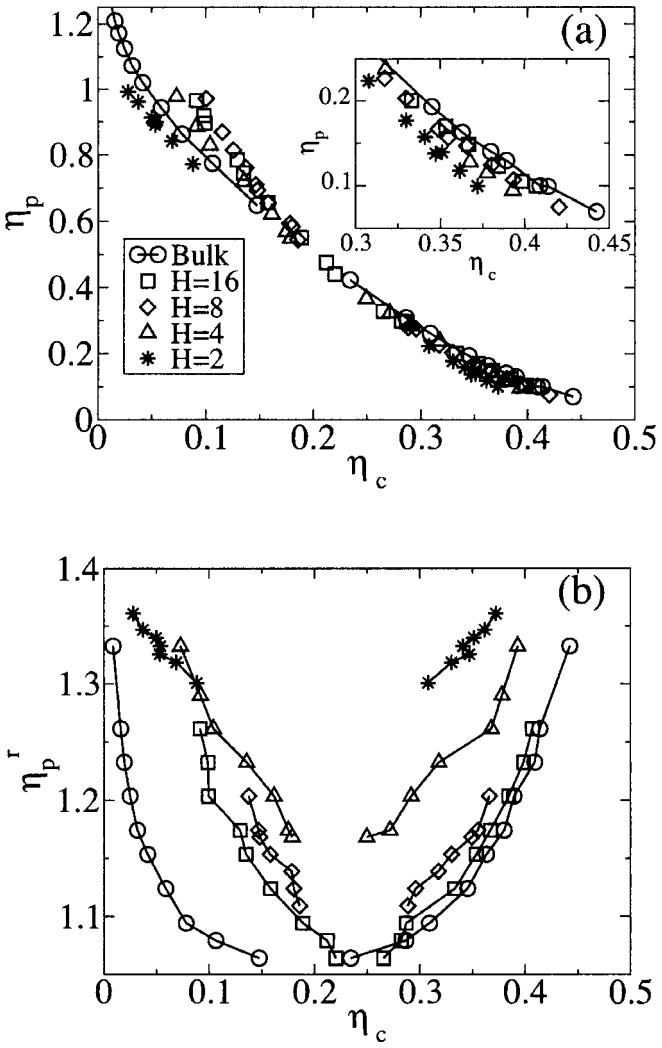

FIG. 7. Phase diagram of colloid-polymer mixtures confined between two hard walls with distances $H/\sigma_c=\infty$(bulk),16,8,4,2. Solid lines are a guide for the eye. (a) Polymer packing fraction η_p, colloid packing fraction η_c representation. Inset: Blowup of the high η_c region of the binodal. (b) Polymer reservoir packing fraction η_p^r, colloid packing fraction η_c representation.

walls [see Figs. 8(a) and 8(c)]. The adsorption of colloids at the walls is due to the depletion attraction, which was also observed in the AOV model. However, the thickness of the liquid layer was in that case much smaller than in the present case and the shift in gas density is less pronounced.[27,31]

Figure 9 displays the phase diagram in the polymer chemical potential μ_p, colloid chemical potential μ_c representation. These variables do not depend on the definition of the volume and are, therefore, independent of the wall separation distance. This is the ideal representation to compare the binodals for different wall separation distances. The binodals collapse to a single line because of the thermodynamic equilibrium conditions of the gas-liquid coexistence. Regions above the binodal are gaslike, while regions below the binodal are liquidlike. We find a shift of the binodals toward higher polymer chemical potential and smaller colloid chemical potential indicating the occurrence of capillary condensation. Our estimates for the critical points are reported in Table IV.

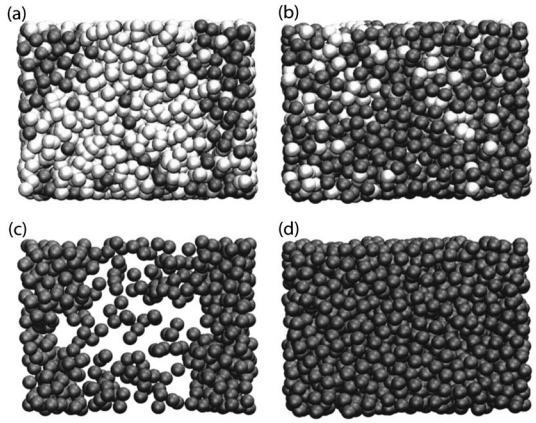

FIG. 8. Typical configurations from computer simulations of the [(a) and (c)] coexisting gas and [(b) and (d)] liquid phase for the confined system with separation distance $H/\sigma_c=16$ and chemical potentials $\mu_c=10.38$ and $\mu_p=5.6$ ($\eta_p^r=1.086$). Colloids are dark gray and polymers are light gray. For clarity (c) and (d) display the same configurations of (a) and (b), respectively, without the polymers.

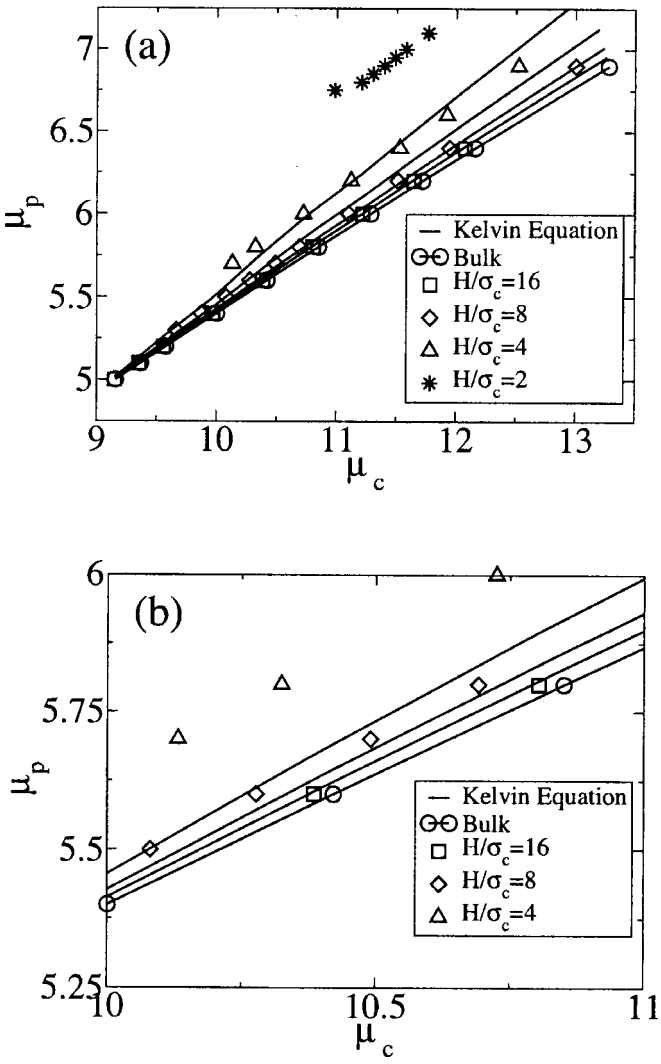

FIG. 9. Phase diagram of colloid-polymer mixtures confined between two hard walls with distances $H/\sigma_c=\infty,16,8,4,2$ in the polymer chemical potential μ_p, colloid chemical potential μ_c representation. In (b), we show a blowup of the phase diagram. For clarity, the results of $H/\sigma_c=2$ are not shown.

TABLE IV. Critical values of the polymer reservior packing fraction η_p^r, colloid packing fraction η_c, and chemical potentials μ_p and μ_c for wall separation distances $H/\sigma_c=\infty$, 16, 8, 4, and 2.

H/σ_c	$(\eta_p^r)_{cr}$	$(\eta_c)_{cr}$	$(\mu_p)_{cr}$	$(\mu_c)_{cr}$
∞	1.06(5)	0.192(5)	4.99(5)	9.23(5)
16	1.08(5)	0.243(5)	5.10(5)	9.45(5)
8	1.09(5)	0.235(5)	5.16(5)	9.50(5)
4	1.17(5)	0.219(5)	5.72(5)	10.25(5)
2	1.27(5)	0.199(5)	6.43(5)	10.64(5)

Also shown in Fig. 9 are the predictions of the Kelvin equation[31]

$$\mu_c = \mu_c^{\text{bulk}} + \frac{2}{h}(\gamma_{\text{wl}} - \gamma_{\text{wg}})\frac{\rho_c^l - \rho_c^g}{(\rho_c^l - \rho_c^g)^2 + (\rho_p^l - \rho_p^g)^2},$$

$$\mu_p = \mu_p^{\text{bulk}} + \frac{2}{h}(\gamma_{\text{wl}} - \gamma_{\text{wg}})\frac{\rho_p^l - \rho_p^g}{(\rho_c^l - \rho_c^g)^2 + (\rho_p^l - \rho_p^g)^2}. \quad (14)$$

The predictions of the Kelvin equation are in good agreement with the simulation results for $H/\sigma_c=16$ and 8 but underestimate the shift for $H/\sigma_c=4$ and 2.

In order to compare the results with those for the AOV model, we scale the binodals by the bulk critical points $(\mu_p)_{\text{cr}}^{\text{bulk}}$ and $(\mu_c)_{\text{cr}}^{\text{bulk}}$, reported in Table IV. Figures 10(a) and 10(b) show that the shift of the binodals and critical points is smaller for the model with interacting polymers than for the AOV model studied in Refs. 27 and 31 for all state points considered. As shown in Fig. 5, the difference $\rho_c^l - \rho_c^g$ between the colloid packing fractions of the liquid and the gas at coexistence is smaller for the interacting polymers than for the AOV model for low η_p^r but larger for high η_p^r. On the other hand, Figs. 10(a) and 10(b) show that the shift in chemical potential is always smaller for the interacting polymers than for the AOV model. Therefore, we deduce from Eq. (14) that the difference $\gamma_{\text{wl}} - \gamma_{\text{wg}}$ (liquid-wall and gas-wall interfacial tensions at coexistence) is smaller for the interacting polymer model.

Moncho-Jorda *et al.*[47] have shown that at constant η_p^r, the excluded volume interactions increase the difference in wall tensions. This is not in contrast with our findings because for capillary condensation, we need to consider the difference in wall tensions at bulk coexistence, that is, at different η_p^r for the AOV model and the interacting polymer model.

V. CONCLUSIONS

We have investigated bulk and confined colloid-polymer mixtures, using Monte Carlo simulations. Colloids are treated as hard spheres, while polymers were described as soft repulsive spheres. Colloid-polymer, polymer-polymer, and wall-polymer density-dependent interactions were described by the coarse-grained potentials derived in Ref. 48. We find a bulk phase behavior consistent with the findings of Bolhuis *et al.*[51] Our results for the bulk phase behavior are also similar to those for the AOV model with interacting polymers[42] but here, the binodal line lies at higher polymer packing fractions; i.e., the number of polymers needed for the demixing transition is larger. These results are in agreement with the findings of other authors.[44,45,51,55] The comparison of our phase diagram with experiments[12] is found to be poor for the size ratio $q=1.05$ considered here. This is surprising, since the same interaction potentials provided good agreement with experiments[60] at a smaller size ratio.[51] In fact, this discrepancy can be explained by considering the results of Wijting *et al.*[59] on depletion potential measurements on the same colloid-polymer mixtures that were used in the phase behavior experiments. These measurements concluded that the depletion attraction was smaller than expected, probably due to polymer adsorption on the surface of the colloids.

On the other hand, better agreement is found for the gas-liquid interfacial tension when compared to the experiments of Aarts *et al.*[21] for the same system. Our results show

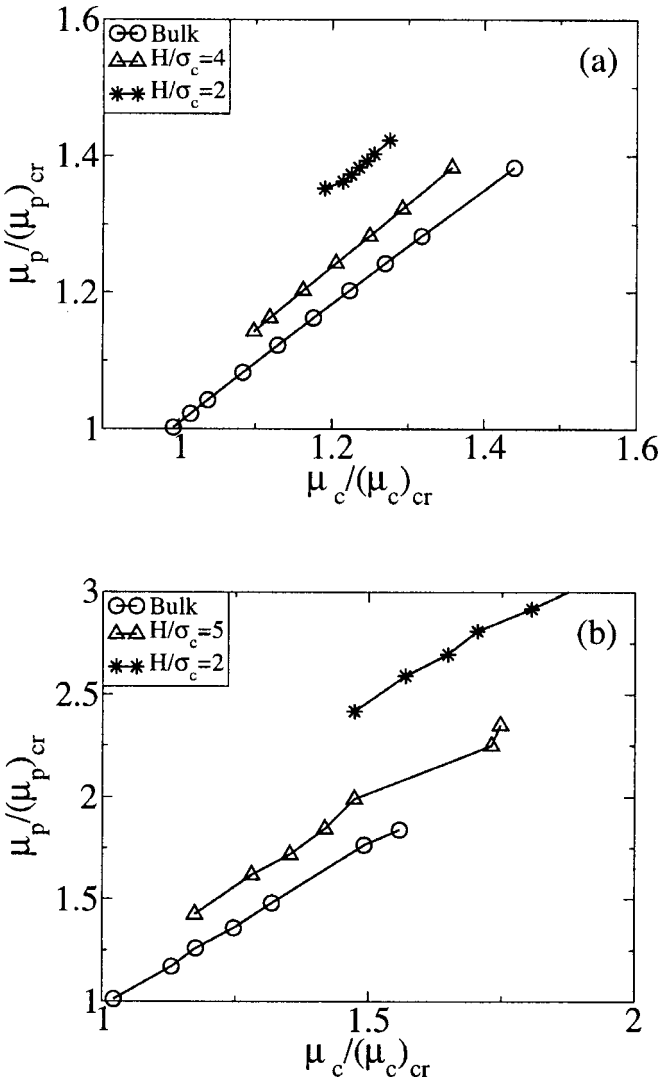

FIG. 10. Phase diagram of colloid-polymer mixtures confined between two hard walls in the polymer chemical potential $\mu_p/(\mu_p)_{\text{cr}}^{\text{bulk}}$, colloid chemical potential $\mu_c/(\mu_c)_{\text{cr}}^{\text{bulk}}$ representation. (a) $H/\sigma_c=\infty$, 4, and 2 for the model discussed in this paper. (b) $H/\sigma_c=\infty$, 5, and 2 for the AOV model. Results are taken from Ref. 31.

that the gas-liquid interfacial tension is smaller for the interacting polymers than for the AOV model. This is in agreement with the works of others on colloid-polymer mixtures with interacting polymers.[40,45,47,55] Both the square gradient approximation and the DFT provide a good description of the simulation results.

In addition, we studied the phase behavior of the mixture confined between two parallel hard walls with separation distances $H/\sigma_c=16$, 8, 4, and 2. We find that the hard walls induce capillary condensation and that the theoretical predictions of the Kelvin equation are in reasonable agreement with the simulation results for $H/\sigma_c=16$ and 8 but underestimate the binodal shifts for $H/\sigma_c=4$ and 2. Compared to the AOV model, the excluded volume interactions suppress the capillary condensation. This implies that the effect can only be observed at state points close to bulk coexistence and that smaller plate separations are needed to induce capillary condensation for fixed supersaturation compared with noninteracting polymers. In other words, the Kelvin length is smaller for interacting polymers than for the AOV model. In addition, we observed the formation of rather thick wetting layers at the largest wall separation we studied. This effect seems to be enhanced by the presence of the excluded volume interactions. At large wall separations, the wetting layers provide an effective confinement $H-2t$, with t the thickness of the wetting layer, as was recognized by Derjaguin,[61] which increases effectively the Kelvin length[30] for the colloid-polymer mixtures with excluded volume interactions. The influence of excluded volume interactions on the wetting properties of colloid-polymer mixtures is currently under investigation.

ACKNOWLEDGMENTS

We thank Remco Tuinier for discussions and Arturo Moncho Jordá and Dirk G.A.L. Aarts for their interfacial tension data. This work is part of the research program of the Stichting voor Fundamenteel Onderzoek der Materie (FOM) that is financially supported by the Nederlandse Organisatie voor Wetenschappelijk Onderzoek (NWO). We thank the Dutch National Computer Facilities Foundation for granting access to the LISA supercomputer. NWO-CW is acknowledge for the TOP-CW funding.

[1] W. C. K. Poon, J. Phys.: Condens. Matter **14**, R859 (2002).
[2] R. Tuinier, J. Rieger, and C. G. de Kruif, Adv. Colloid Interface Sci. **103**, 1 (2003).
[3] J. M. Brader, R. Evans, and M. Schmidt, Mol. Phys. **101**, 3349 (2003).
[4] P. N. Pusey and W. van Megen, Nature (London) **320**, 340 (1986).
[5] S. Asakura and F. Oosawa, J. Chem. Phys. **22**, 1255 (1954).
[6] S. Asakura and F. Oosawa, J. Polym. Sci. **33**, 183 (1958).
[7] A. Vrij, Pure Appl. Chem. **48**, 471 (1976).
[8] A. P. Gast, C. K. Hall, and W. B. Russel, J. Colloid Interface Sci. **96**, 251 (1983).
[9] H. N. W. Lekkerkerker, W. C. K. Poon, P. N. Pusey, A. Stroobants, and P. Warren, Europhys. Lett. **20**, 559 (1992).
[10] E. J. Meijer and D. Frenkel, J. Chem. Phys. **100**, 6873 (1994).
[11] M. Dijkstra, J. M. Brader, and R. Evans, J. Phys.: Condens. Matter **11**, 10079 (1999).
[12] E. H. A. de Hoog and H. N. W. Lekkerkerker, J. Phys. Chem. B **103**, 5274 (1999).
[13] B.-H. Chen, B. Payandeh, and M. Robert, Phys. Rev. E **62**, 2369 (2000).
[14] M. Schmidt, H. Löwen, J. M. Brader, and R. Evans, Phys. Rev. Lett. **85**, 1934 (2000).
[15] M. Schmidt, H. Löwen, J. M. Brader, and R. Evans, J. Phys.: Condens. Matter **14**, 9353 (2002).
[16] R. L. C. Vink and J. Horbach, J. Chem. Phys. **121**, 3253 (2004).
[17] J. M. Brader, M. Dijkstra, and R. Evans, Phys. Rev. E **63**, 041405 (2001).
[18] J. M. Brader, R. Evans, M. Schmidt, and H. Löwen, J. Phys.: Condens. Matter **14**, L1 (2002).
[19] M. Dijkstra and R. van Roij, Phys. Rev. Lett. **89**, 208303 (2002).
[20] W. K. Wijting, N. A. M. Besseling, and M. A. Cohen Stuart, J. Phys. Chem. B **107**, 10565 (2003).
[21] D. G. A. L. Aarts, J. H. van der Wiel, and H. N. W. Lekkerkerker, J. Phys.: Condens. Matter **15**, S245 (2003).
[22] W. K. Wijting, N. A. M. Besseling, and M. A. Cohen Stuart, Phys. Rev. Lett. **90**, 196101 (2003).
[23] D. G. A. L. Aarts, J. Phys. Chem. B **109**, 7407 (2005).
[24] A. Fortini, M. Dijkstra, M. Schmidt, and P. P. F. Wessels, Phys. Rev. E **71**, 051403 (2005).
[25] P. P. F. Wessels, M. Schmidt, and H. Löwen, J. Phys.: Condens. Matter **16**, S4169 (2004).
[26] P. P. F. Wessels, M. Schmidt, and H. Löwen, J. Phys.: Condens. Matter **16**, L1 (2004).
[27] M. Schmidt, A. Fortini, and M. Dijkstra, J. Phys.: Condens. Matter **15**, 3411 (2003).
[28] T.-C. Lee, J.-T. Lee, D. Pilaski, and M. Robert, Physica A **329**, 411 (2003).
[29] M. Schmidt, A. Fortini, and M. Dijkstra, J. Phys.: Condens. Matter **16**, S4159 (2004).
[30] D. G. A. L. Aarts and H. N. W. Lekkerkerker, J. Phys.: Condens. Matter **16**, S4231 (2004).
[31] A. Fortini, M. Schmidt, and M. Dijkstra, Phys. Rev. E **73**, 051502 (2006).
[32] R. L. C. Vink, K. Binder, and J. Horbach, Phys. Rev. E **73**, 056118 (2006).
[33] R. L. C. Vink, A. D. Virgiliis, J. Horbach, and K. Binder, Phys. Rev. E **74**, 031601 (2006).
[34] A. D. Virgiliis, R. L. C. Vink, J. Horbachand, and K. Binder, Europhys. Lett. **77**, 60002 (2007).
[35] M. Schmidt and A. R. Denton, Phys. Rev. E **65**, 061410 (2002).
[36] A. R. Denton and M. Schmidt, J. Phys.: Condens. Matter **14**, 12051 (2002).
[37] A. R. Denton and M. Schmidt, J. Chem. Phys. **122**, 244911 (2005).
[38] A. Fortini, M. Dijkstra, and R. Tuinier, J. Phys.: Condens. Matter **17**, 7783 (2005).
[39] M. Schmidt, A. R. Denton, and J. M. Brader, J. Chem. Phys. **118**, 1541 (2003).
[40] R. L. C. Vink and M. Schmidt, Phys. Rev. E **71**, 051406 (2005).
[41] M. Schmidt, M. Dijkstra, and J.-P. Hansen, Phys. Rev. Lett. **93**, 088303 (2004).
[42] D. G. A. L. Aarts, R. Tuinier, and H. N. W. Lekkerkerker, J. Phys.: Condens. Matter **14**, 7551 (2002).
[43] J. M. Brader and R. Evans, Europhys. Lett. **49**, 678 (2000).
[44] A. Moncho-Jorda, B. Rotenberg, and A. A. Louis, J. Chem. Phys. **119**, 12667 (2003).
[45] D. G. A. L. Aarts, R. P. A. Dullens, H. N. W. Lekkerkerker, D. Bonn, and R. van Roij, J. Chem. Phys. **120**, 1973 (2004).
[46] A. A. Louis, P. G. Bolhuis, E. J. Meijer, and J.-P. Hansen, J. Chem. Phys. **117**, 1893 (2002).
[47] A. Moncho-Jorda, J. Dzubiella, J.-P. Hansen, and A. A. Louis, J. Phys. Chem. B **109**, 6640 (2005).
[48] P. G. Bolhuis and A. A. Louis, Macromolecules **35**, 1860 (2002).
[49] A. A. Louis, P. G. Bolhuis, J. P. Hansen, and E. J. Meijer, Phys. Rev. Lett. **85**, 2522 (2000).
[50] P. G. Bolhuis, A. A. Louis, J. P. Hansen, and E. J. Meijer, J. Chem. Phys. **114**, 4296 (2001).
[51] P. Bolhuis, A. A. Louis, and J.-P. Hansen, Phys. Rev. Lett. **89**, 128302 (2002).
[52] A. Jusufi, J. Dzubiella, C. N. Likos, C. von Ferber, and H. Löwen, J. Phys.: Condens. Matter **13**, 6177 (2001).
[53] J. Dzubiella, C. N. Likos, and H. Lowen, J. Chem. Phys. **116**, 9518 (2002).
[54] R. Rotenberg, J. Dzubiella, A. A. Louis, and J.-P. Hansen, Mol. Phys. **102**, 1 (2004).
[55] R. L. C. Vink, A. Jusufi, J. Dzubiella, and C. N. Likos, Phys. Rev. E **72**, 030401(R) (2005).

[56] P. Virnau and M. Müller, J. Chem. Phys. **120**, 10925 (2004).
[57] K. Binder, Phys. Rev. A **25**, 1699 (1982).
[58] H. N. W. Lekkerkerker, Colloids Surf. **51**, 419 (1990).
[59] W. K. Wijting, W. Knobon, N. A. M. Bossoling, F. A. M. Leermakers, and M. A. Cohen Stuart, Phys. Chem. Chem. Phys. **6**, 4432 (2004).
[60] S. Ramakrishnan, M. Fuchs, K. S. Schweizer, and C. F. Zukoski, J. Chem. Phys. **116**, 2201 (2002).
[61] B. V. Derjaguin, Acta Physicochim. URSS **12**, 181 (1940).